

# Hybrid pulse-burst / cross-correlation DGV for high-speed flow measurements at 100 kHz

Ross A. Burns<sup>1,\*</sup>, Tim W. Fahringer, Jr.<sup>2</sup>, Paul M. Danehy<sup>2</sup>

1: National Institute of Aerospace, USA

2: NASA Langley Research Center, USA

\* Correspondent author: ross.a.burns@nasa.gov

**Keywords:** DGV, Pulse-burst, Supersonic, Hypersonic

## ABSTRACT

Hybrid pulse-burst Doppler global velocimetry (PB-DGV)/pulse-burst, cross-correlation DGV (PB-CC-DGV) was demonstrated for the first time in the NASA Langley 4-foot Supersonic Unitary Plan Wind Tunnel, allowing simultaneous acquisition of mean and instantaneous high-repetition-rate velocity fields. The technique was used to make planar velocity measurements across an oblique shockwave generated by a large splitter plate set at a  $-2^\circ$  angle of attack in a Mach 2.4 flow. Sequences of more than 100 consecutive instantaneous velocity images were obtained at a rate of 100 kHz. Velocity fields from both aspects of the hybrid measurement indicated errors less than 1-percent of anticipated velocities. Likewise, all assessments of measurement precision were approximately 1.6-percent of the local velocities. Additional demonstrations in different flowfields including a subsonic axi-symmetric jet and a supersonic Mars reentry vehicle model further illustrate the utility of the new hybrid method.

---

## 1. Introduction

Nonintrusive, off-body velocity measurements are often challenging to conduct in large-scale wind tunnel facilities. While numerous methods have been developed and optimized for small-scale facilities, such as particle image velocimetry (PIV) and Doppler global velocimetry (DGV), the application of most of these techniques in large-scale facilities continues to be difficult due to the scale and other detrimental aspects of these facilities, such as vibrations and limited optical access.

DGV has previously been shown to be an effective velocimetry method in the NASA Langley Unitary Plan Wind Tunnel (UPWT), (Meyers, 1995) where the capability of seeding particles suitable for PIV does not currently exist and optical access appropriate for most molecular methods is not available. Though its uses are sparse, DGV is currently viewed as the most appropriate non-intrusive, off-body velocimetry technique for use in this facility. Numerous advancements have been made to the original DGV method over the years to improve the overall fidelity of the technique. Fischer provides an overview of many of these variations on the original

technique. (Fischer 2017) The concept of cross-correlation Doppler global velocimetry (CC-DGV) was developed by Cadel and Lowe. (Cadel 2015) In this variant of the DGV concept, rather than utilizing a single laser frequency as in the original DGV concept or multiple specific frequencies such as other variants, (Charrett 2004)(Müller 2007) the laser frequency is scanned to many discrete frequencies across an absorption feature in a typical optical filter (gaseous  $I_2$  or equivalent). By measurement of the absorption at each of these frequencies, a Doppler-shifted absorption spectrum can be constructed. Comparing these measured spectra with a zero-velocity reference through cross-correlation allows a Doppler shift to be measured and the velocity inferred. This measurement is intrinsically an average measurement as originally conceived due to the continuous-wave laser employed, the slow rate of frequency scanning, and the long camera exposures needed to acquire sufficient signal. However, since the technique relies on many camera exposures and isn't limited to a small spectral region of an absorption feature, many of the shortcomings of the DGV concept are avoided, including the limited velocity measurement range (requiring a priori knowledge of the velocity) and the dependence on absolute image intensity. Lowe et al. recently applied a three-component CC-DGV system in the NASA Langley UPWT to study the flow over a SLS model during booster separation. (Lowe 2019)

A new version of CC-DGV was devised by Fahringer et al. called pulse-burst, cross-correlation DGV (PB-CC-DGV), in which a pulse-burst laser with frequency scanning capabilities was used in conjunction with high-speed cameras to replicate the frequency-scanning and data acquisition used in CC-DGV. (Fahringer 2020) This high-speed variant reduced the measurement time from a few minutes to 10 ms or less while maintaining the numerous advantages associated with CC-DGV. PB-CC-DGV was successfully employed in UPWT to make measurements in both the flow across an oblique shock (Burns 2020) and in numerous reentry flowfields. (Burns 2021) A recent study by Saltzman et al. examined the effects of velocity fluctuations in applying this technique in turbulent flows. (Saltzman 2022) However, one of the limitations of PB-CC-DGV is that it remains an average measurement; the velocities measured are averaged over the duration of a burst of pulses. While valuable in this form, making high-repetition-rate (10s or 100s of kHz) measurements in high-speed flow environments is still a desirable capability that this technique forgoes. In this paper, a framework is established and demonstrated, which allows for the simultaneous acquisition of both mean velocities through PB-CC-DGV and instantaneous, high-speed velocity measurements through pulse-burst DGV (PB-DGV, originally done by Thurow (Thurow 2005)) with the same measurement system(s). Hybrid PB/CC-DGV is demonstrated in the flow across an oblique shock. These measurements are compared to each other and assessed for accuracy and temporal behavior. Further demonstrations of the hybrid technique are also presented, showing the utility of this technique across of range of flow conditions. This paper is

structured as follows: after this introduction, the measurement principle is explained, followed by information about the experimental setup, data analysis methods, the results and discussion, and finally the conclusions.

## 2. Measurement Principle

A typical pair of measured absorption spectra from PB-CC-DGV (both reference and signal) are shown in Fig. 1. Refer to (Burns 2021) and (Burns 2022) for an explanation of how these spectra were acquired. In PB-CC-DGV, the Doppler shift for a given measurement location is extracted by performing cross-correlation between these two spectra after some numerical manipulation. In this case, the 1000 or so pulses that comprise the laser burst are each at a slightly different, but known, frequency, and a single Doppler shift is extracted for this measurement location. The idea behind hybrid PB/CC-DGV is that while all these data can be collapsed into a single averaged measurement, certain regions of the absorption well contain the instantaneous Doppler shift information commonly used for making fixed-frequency DGV measurements (see for example Herring et al. (2009) and/or Thurow et al. (2005)). Specifically, any region in the Doppler shifted spectrum in which intensity/transmission changes are not ambiguous (regions with rapid changes in absorption) can be used for instantaneous DGV.

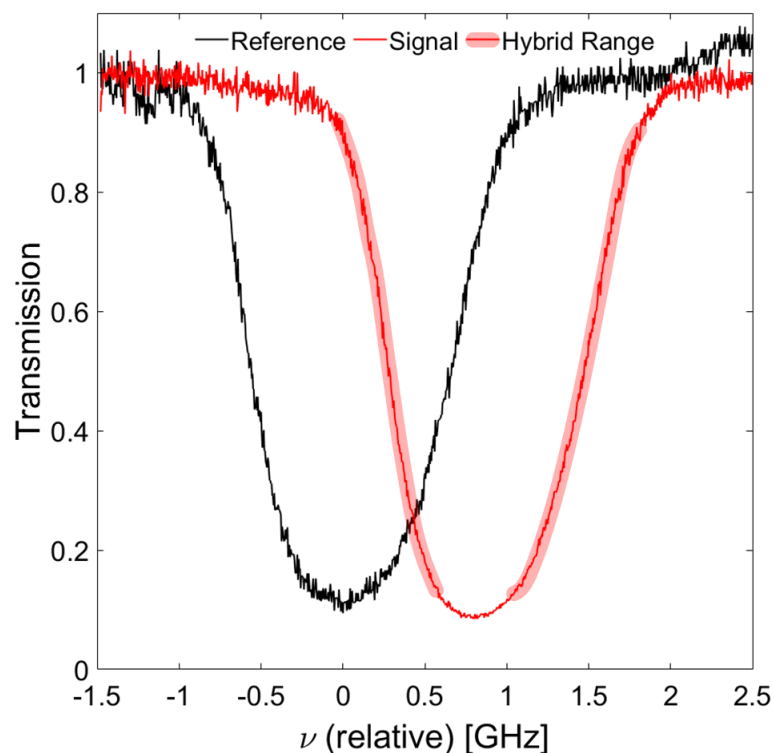


**Fig. 1** Sample absorption spectra from PB-CC-DGV. Highlighted regions indicate those usable for the hybrid pb/cc-dgv.

In Fig. 1, the regions on the Doppler-shifted (signal) spectrum from roughly 0 to 0.5 GHz and 1.1 to 1.5 GHz could be used for this purpose (highlighted in red in Fig. 1), or roughly 250 of the 1000 laser pulses. Rather than using a fixed reference frequency as is the case for fixed-frequency DGV, the reference frequency in this new method is continuously changing from pulse to pulse and being actively monitored. With knowledge of the reference frequency and the Doppler-shifted frequency at the measurement location, the instantaneous signal in the images can be interpreted as a Doppler shift measurement, as would be done in standard DGV. Using this method, a high-precision, large measurement range Doppler shift measurement can be constructed by using the CC-DGV method, while two,  $\sim 125$  pulse-long contiguous bursts of high-repetition-rate DGV are extracted from the same data set, allowing frequency content and high-speed fluctuations to be observed as well.

### 3. Experimental Details

#### A. Experimental Facility and Test Article

The tests were conducted in the 4-Foot Supersonic Unitary Plan Wind Tunnel (UPWT), a continuous-flow supersonic test facility located at NASA Langley Research Center in Hampton, VA. The Mach number of the facility is continuously variable from 1.47 to 4.64, achieved by utilizing a sliding nozzle block configuration. Two different test sections account for the full range of Mach numbers. Test Section I covers Mach numbers in the range of 1.47 to 2.87, while Test Section II accommodates Mach numbers ranging from 2.29 to 4.64. These tests were conducted in Test Section II. Both test sections have cross-sectional dimensions of 1.32 m by 1.22 m. Test conditions were constant across all tests, with a nominal Mach number of 2.399, a unit Reynolds number of  $3.3 \times 10^6/\text{m}$ , a total temperature of 325 K, and a total pressure of 41 kPa. The flow was seeded for DGV by injecting liquid water downstream of the test section. In circulating through the facility, a fog of ice crystal develops in the nozzle and passes into the test section; this fog was used as the scattering medium. Optical access to the test section was afforded by a series of vertical windows arranged along each sidewall. Each window was approximately 0.13 m wide and separated from the next by a 0.03 m steel spar, which were approximately 0.23 m deep. A schematic showing these windows can be seen in the test section diagram in Fig. 2, along with the test section optics and camera configuration. The oblique shock for these tests was generated with a large splitter-plate oriented horizontally at the vertical mid-line of the test section. A sketch of this model can be seen in Fig. 2. The splitter-plate was declined by  $2^\circ$  to generate the weak oblique shock on its top surface. This model was used previously by Herring et al. (2009) making similar

measurement assessments, as well as Burns et al. in experiments accompanying the present studies. (Burns 2021)

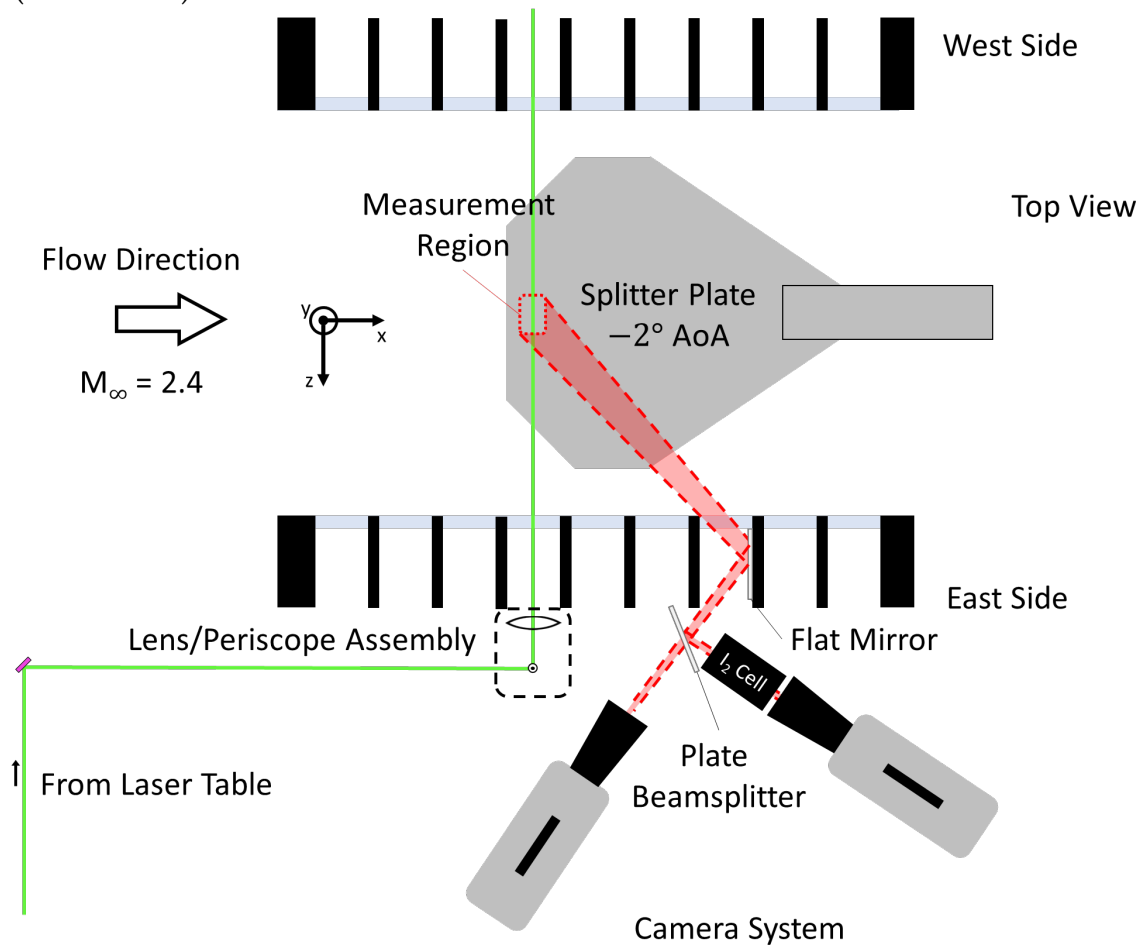


Fig. 2 Top-view diagram of experimental setup around test section.

## B. Laser and Optical Systems

### 1. Laser

The laser used in these studies was a burst-mode, master oscillator, pulsed amplifier system (Spectral Energies QuasiModo). The laser utilized an external cavity diode laser (ECDL, Sacher LiON series) as a seed laser, which allowed the laser frequency to be rapidly scanned through variation of the laser diode current (or through piezo actuation, alternatively). The operating frequency of the laser was set to 100 kHz, while the burst duration and period were 10 ms and 12 s, respectively. The second harmonic of this Nd:YAG system was used. The center wavelength ( $\lambda$ ) was set to 532.217 nm to capture the desired  $I_2$  absorption features, and the linewidth is specified between 60 and 100 MHz at 1064 nm. Figure 3 presents a schematic of the principal laser system. The output from the main amplifier head is divided into two pathways: a diagnostic leg and the main experimental leg. The diagnostic leg, which was sampled by taking the small fraction of light (less than 1 percent) that passed through a high-reflectivity mirror, housed the diagnostic systems

used to characterize the laser output. The main experimental leg first passed through a variable attenuator ( $\lambda/2$ -plate + plate polarizer) and then a one-to-one telescope with a small (500  $\mu\text{m}$ ) iris at its focus, which was used to help limit beam steering associated with thermal lensing during the burst. This portion of the laser system then transmitted the beam over to the wind tunnel test section.

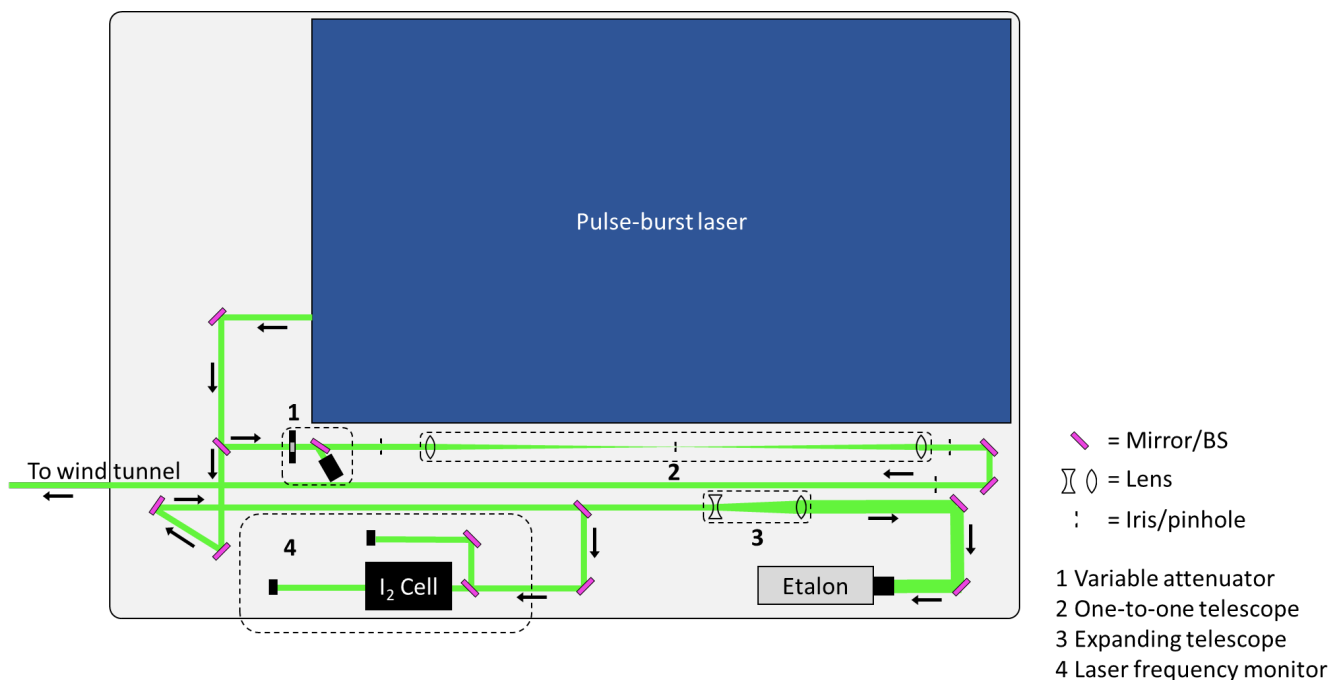


Fig. 3 Diagram of principal laser setup.

## 2. Laser frequency monitor (LFM)

The LFM acted as a zero-velocity reference for comparison with Doppler-shifted spectra. The device allowed an instantaneous measurement of optical absorption. The LFM consisted of two photodiodes (Thorlabs DET210), each fitted with a laser line filter (passing 532 nm) and a lens / optical diffuser system to minimize the effects of spatial variations in the laser profile or position. The laser beam in the diagnostics leg (containing less than one percent of the total laser energy) is sampled using two partially reflective mirrors, one 20-percent and one 50-percent, to reduce the overall input energy to the LFM. This input energy is divided into two paths using a non-polarizing 50-percent beamsplitter, each path leading to one photodiode. One path propagates unperturbed, while the other passes through a gaseous  $\text{I}_2$  cell (ISSI I2M-5, cell pressure 1 Torr at 40  $^{\circ}\text{C}$ ), which was held at a constant 70  $^{\circ}\text{C}$  by a thermoelectric controller (Digi-Sense TC5000). The overall intensity of the laser was adjusted by placing absorptive neutral-density (ND) filters on the front of the system, while the balance of the channels was accomplished by placing lower-density ND filters on each path. The beam paths of the LFM system were enclosed in one-inch tube system

components to prevent contamination from ambient scattered light. The output from the photodiodes was captured using an oscilloscope (Tektronix DPO7354) with custom data acquisition software to automatically acquire the traces from multiple sequential bursts, allowing the system to run for 10s of minutes without human input.

### 3. Laser etalon

A confocal Fabry-Pérot etalon (Burleigh) with a free-spectral range of 750 MHz was used to monitor relative changes in the laser frequency. In combination with the LFM, the etalon allowed the zero-velocity absorption spectra to be correctly scaled in the frequency domain and corrected for errors associated with nonlinear scanning. The input to the etalon from the diagnostic leg of the laser system was diametrically expanded by a factor of 6 using a telescopic lens pair (-50-mm and +300-mm spherical lenses) and attenuated using absorptive ND filters to adjust the intensity prior to entering the etalon. Data from the etalon was acquired using the same 4-channel oscilloscope as the LFM. Note that the fourth channel of the oscilloscope was used for one of several system inputs such as the waveform input to the ECDL, one camera's exposure positive signal, or the current out of the ECDL, depending on what was needed at the time.

### 4. Test section optics

Prior to entering the test section, the beam was transmitted above the model using a periscopic mirror pair. The beam was expanded into a collimated sheet approximately 63 mm tall using a pair of lenses (-75-mm cylindrical lens and +1-m spherical). This sheet then passed through the test section at a declined angle ( $5^\circ$ ) to prevent etaloning by the window, the surfaces of which are highly parallel to allow for Schlieren imaging in the facility. The sheet skimmed over the surface of the plate and impinged outside the imaging field-of-view. The remaining sheet was captured by a beam stop after passing outside of the test section. The approximate position of these optics can be seen in Fig. 2. The sheet was positioned 127 mm downstream of the leading edge of the plate.

### 5. Imaging System

The camera imaging configuration by the test section is shown in Fig. 2. The scattering was captured using a dual-imaging system. Two high-speed CMOS (coupled metal-oxide semiconductor) cameras (Photron SA-Z) equipped with 185-mm,  $f/2.8$  lenses were oriented orthogonally to each other. One camera (signal channel) imaged through a gaseous  $I_2$  filter (ISSI I2M-5, identical to the one used in the LFM), while the other served as a reference channel. Both cameras imaged through a 50-percent, non-polarizing, plate beamsplitter and were situated to

have the same field-of-view. A flat mirror mounted to one of the spars 0.75 m downstream of the laser sheet was used to direct the entire field-of-view to the center of the test section, imaging at an approximate angle of  $42^\circ$  from the streamwise direction. In this configuration, principally backward-oriented laser scatter was viewed, which increased the magnitude of the observed Doppler shifts at the expense of lower signals compared to forward scatter.

Both cameras were operated at 100 kHz and had a magnification of  $210 \mu\text{m}/\text{pixel}$ . Each burst of the laser resulted in approximately 1000 images of data per camera. Furthermore, the camera fields-of-view were approximately 100 mm wide by 100 mm tall, with data present in the central 75 mm wide by 50 mm tall.

## 4. Data Analysis

### A. PB-CC-DGV

The first stages in the data analysis for the hybrid PB/CC-DGV technique is to complete the original PB-CC-DGV technique. The complete details on this analysis can be found in Burns (2020, 2021) and will not be recounted in this paper. However, as a summary of all steps, raw images are first corrected for image distortion and spatially mapped onto each other. Concurrently, data from the LFM and etalon are used to generate the zero-velocity reference absorption spectrum. Pixelwise, Doppler-shifted absorption spectra are then generated from the image data, and the Doppler shifts are evaluated by performing cross-correlation between these spectra and the reference.

### B. Spectral Conditioning

Following the completion of PB-CC-DGV, the reference (LFM) and signal (camera) spectra are saved. Since the reference frequency is known for each image (the reference spectrum having been constructed during the first stages of data analysis), determining instantaneous Doppler shifts is done exclusively using the signal spectra. Before describing that process, first consider Fig. 4, which shows a signal spectrum compared to a theoretical spectrum of the same line generated using the Forkey model. (Forkey 1997) What is apparent from Fig. 4 is that while the profiles of these absorption wells approximately match, the exact shapes differ slightly over the scan range. This observation is true in both the reference and signal spectra. The most likely causes for this discrepancy are the finite laser linewidth and/or imperfect amplification of the seed laser, and inexact matching between the conditions of the simulated and measured spectra, along with the potential for dynamic range limitations and imprecisely matched detector sensitivities. The

broadened spectrum noted in Fig. 4 shows a significant improvement in matching the measured to the simulated spectrum assuming a laser linewidth between 300 and 350 MHz. In performing

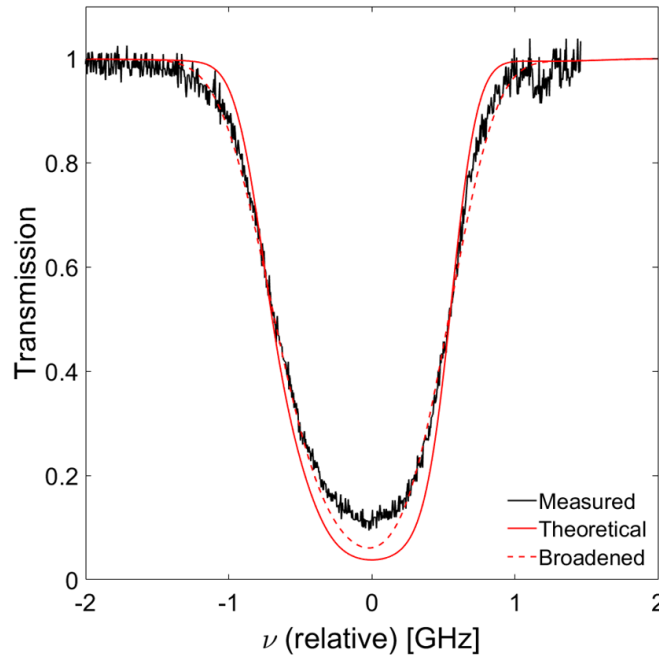


**Fig. 4** Comparison of a measured absorption spectrum with theoretical.

PB-CC-DGV, this deviation from expected spectral behavior is of lesser consequence than in fixed-frequency DGV or the present method. Since the broadening and other effects are imparted to both the reference and signal spectra, and the Doppler shift is determined by means of cross-correlation rather than directly from intensity, the effect is ultimately mitigated. However, to extract instantaneous information from the PB-CC-DGV data, deviations from theory must be accommodated. For these studies, a heavily conditioned version of the absorption spectrum for each pixel is used in evaluating the Doppler shift rather than a theoretical or simulated surrogate. To perform this conditioning, a 20-pt Gaussian smoothing filter is applied twice to the signal spectrum at each pixel to remove experimental noise. Note that the width of this filter is determined by the level of noise in the data and must be adjusted accordingly.

### C. Frequency Determination

After sufficiently conditioning the absorption spectra, Doppler-shifted frequencies are determined through interpolation. The allowable region of the absorption well to be used is first determined. For these data, the transmission limits used in finding the allowable regions for the technique were determined to be  $[0.15, 0.9]$ , and were evaluated on the smoothed signal spectra generated in the previous step. Images corresponding to transmission values in this range were then considered for this method. Note that the use of the low-frequency (downward) or high-frequency (upward)

side of the absorption well had little bearing on this procedure other than reversing the direction of the limits during this initial determination. Also note that since a spatial variation in the Doppler shift will exist in most data, not all pixels in an image will necessarily be considered valid for instantaneous measurement at all times. Rather, the time within the burst when 100+ instantaneous measurements can be obtained may vary around the image, particularly if there is a large dynamic range of velocities within the field of view. Next, using the raw signal spectra (not the smoothed ones), the transmission at each pixel location is determined. The corresponding relative frequency change is then determined by interpolating on the corresponding side (downward or upward) of the smoothed absorption well. The total Doppler shift is then determined by adding the mean Doppler shift initially determined through PB-CC-DGV to the relative Doppler shift determined through interpolation.

#### D. Velocity Evaluation

Velocities are inferred from the measured Doppler shifts identically to PB-CC-DGV. Details on this procedure are given in Burns (2021). To summarize the major steps of this procedure: the relevant measurement vectors, the observation ( $\hat{o}$ ) and laser incidence ( $\hat{i}$ ) are first determined. The  $\hat{o}$  vector is directly extracted from the camera calibration procedure, while the  $\hat{i}$  vector is measured by a combination of manual measurements and evaluation of the fanning angle of the laser from the corrected images. Once these relevant vectors have been determined, the velocity ( $u$ ) is related to the Doppler shift ( $\Delta\nu$ ) through the relation (Eq. 1):

$$\Delta\nu = \frac{\vec{u} \cdot (\hat{o} - \hat{i})}{\lambda} \quad (1)$$

Specific to this data set, it was assumed during this procedure that the Doppler shift resulted solely from the streamwise ( $x$ -) component of velocity. This assumption is robust in the context of these experiments due to the primarily unidirectional flow. With this assumption, the streamwise velocity can be evaluated per Eq. 2:

$$u_x = \frac{\lambda\Delta\nu}{(\hat{o} - \hat{i})_x} \quad (2)$$

Note also that the sensitivity vector was assessed pixelwise and was determined during the initial calibration of the camera system.

## 5. Results and Discussion

Two-dimensional surface plots of streamwise velocity are shown in Fig. 5. Before describing the velocimetry results, the data are arranged as follows: the vertically-oriented laser sheet cuts across

the shockwave approximately 127 mm back from the leading edge of the splitter plate. The results from within the measurement plane show two distinct regions: the pre-shock (higher velocity)

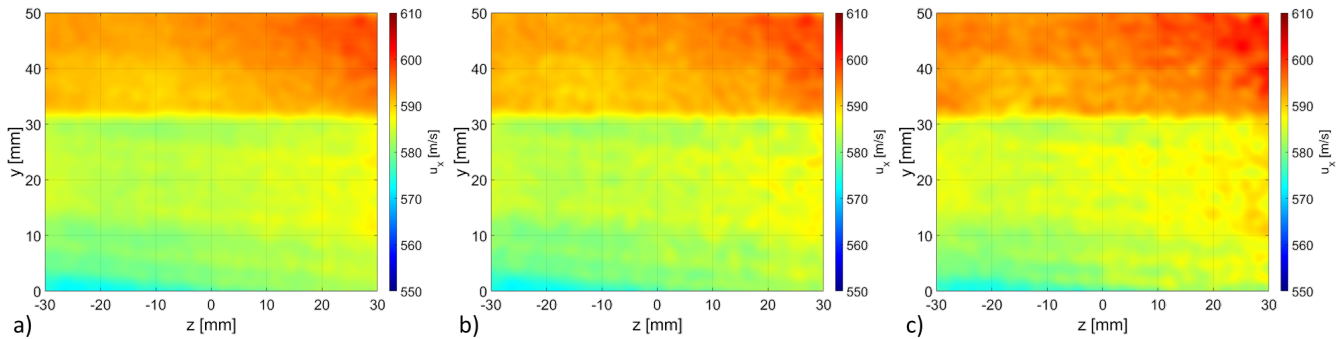


**Fig. 5** Sample streamwise velocity fields acquired using the hybrid PB/CC-DGV in the oblique shock flowfield. a) Mean from original PB-CC-DGV, b) instantaneous velocity field from h-PB/CC-DGV using the downward slope of the absorption well, and c) instantaneous velocity field from h-PB/CC-DGV using the upward slope of the absorption well. All data is from the same laser burst.

region and the post-shock (lower velocity) region, separated by the shockwave at approximately  $y = 31$  mm. Also note that the flow is quite steady and no significant oscillations in the shock position or angle were expected or observed. In Fig. 5a, the original PB-CC-DGV data is shown. As described previously, two distinct flow regions are present corresponding to the pre- and post-shock states. Both regions appear homogeneous aside from minor horizontal striations consistent with variations in the laser beam profile, and a subtle lateral gradient, likely resulting from slight imperfections in the determination of the sensitivity vector and its components. Previous assessments of this PB-CC-DGV dataset indicated measurement errors to be within 0.5 percent of the reference velocities for both the pre- and post-shock regions, and measurement precision to be about 1.4 percent of the freestream velocity.

In comparison to these data, the hybrid PB/CC-DGV appears to perform similarly well. Figures 5b and 5c show instantaneous velocity fields extracted through the hybrid PB/CC-DGV method. Figure 5b utilized the low-frequency side of the absorption well, while 5c utilized the high-frequency side of the well. All data shown in Figure 5 are from the same laser burst. Individually, the velocity fields extracted through this method appear to be noisier (spatially) than the original PB-CC-DGV. This observation is more obvious when looking at multiple consecutive frames of data. Additionally, the shock does appear less uniform and moves slightly, both in space and time. The laser striations and lateral gradient also appear more pronounced in the instantaneous frames. Aside from the instantaneous nature of these data, this behavior is also consistent with the evaluation of the sensitivity vector components. Notably, the vectors are evaluated on a mean basis, and the slight temporal variations will cause deviations from that mean position if some elements of the measurement system are dynamic (e.g., slight motions of the laser

sheet). No drastic differences between the velocity fields evaluated on either side of the absorption well were observed in this data format, though some subtle differences will be discussed in the next section.

To examine the temporal behavior of these data, time traces for several burst have been compiled in Fig. 6 for both the left and right sides of the absorption well. Figure 6 compares three different parameters associated with the shock wave: the raw velocities, the velocity ratio, and the velocity difference. To make these evaluations, a small sampling region was selected from the centerline of the pre- ( $u_1$ , red) and post-shock ( $u_2$ , black) areas, and the velocities within those regions averaged for reporting. In addition to the hybrid velocity data, the corresponding PB-CC-DGV values for each burst are shown, along with the reference value for each parameter. Starting first with the raw velocities, it is seen that the hybrid PB/CC-DGV measurements track closely with the PB-CC-DGV values. The velocities obtained from the low-frequency side of the well generally show slight negative deviations from the PB-CC-DGV, while those obtained on the high-frequency side tend to initially exceed the PB-CC-DGV velocity and trend downward slightly, typically ending less than the PB-CC-DGV values. Globally, deviations from the PB-CC-DGV were less than 5 m/s, or about 1 percent of the expected local velocities. Another apparent trend is that the hybrid PB/CC-DGV mimics the behavior of the PB-CC-DGV. Since these data are both extracted from the same dataset, factors affecting specific bursts will likewise affect both velocity evaluation methods. To reiterate a point made above, one of the main reasons this flow was selected was that it was very steady, and deviations from expected values were most likely the result of the measurement system. Previously noted in Burns (2021), some possible sources for these burst-to-burst variations are related to the use of the pulse-burst laser and include thermal beam steering, beam expansion during laser bursts, and large variations in beam spatial profile and intensity from burst to burst. Improving this technique beyond its current state (and the PB-CC-DGV accordingly) will require some or most of these issues to be addressed. Accuracy ( $\epsilon$ ) for these measurements globally range from 0.84 to 1.02 percent of local velocities, while the measurement precision (assessed as one standard deviation over the complete ensemble) range from 1.56 to 1.70 percent of the local velocities. As anticipated, these values are similar but slightly diminished from the PB-CC-DGV measurements. These results and others are summarized in Table 1.

The other parameters that characterize the shockwave are shown in Figs. 6c-f. Figures 6c and 6d show the measured velocity ratio across the shockwave, and Figs. 6e and 6f show the velocity difference across the shock. These parameters are more sensitive than the raw velocities because of their smaller magnitudes. The hybrid PB/CC-DGV measurements, while still tracking with the PB-CC-DGV measurements, show significantly more temporal variability than the raw

velocities suggest. Certain bursts of data show relatively minor fluctuations (for example,  $\sigma = 0.001$  in the velocity ratio and 0.5 m/s in velocity difference), while others are more substantial (for example,  $\sigma = 0.005$  in velocity ratio and 6 m/s in velocity difference), though little difference is observed in the raw velocities. While most bursts indicate temporal behavior consistent with

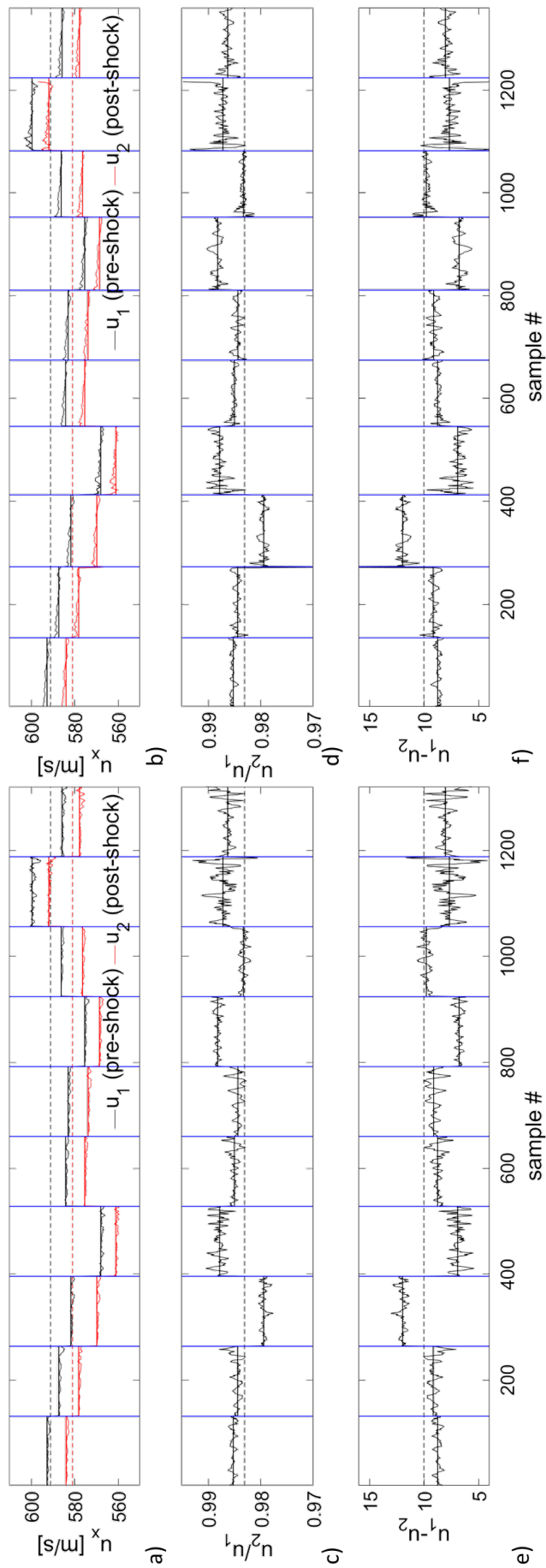


**Fig. 6** Measured instantaneous velocities compared with their mean and expected values. a) and b) Pre- (black) and post-shock (red) velocities, c) and d) velocity ratio across the shockwave, and e) and f) velocity difference across the shockwave. Solid horizontal lines indicate the mean value acquired using PB-CC-DGV, while dashed horizontal lines represent the expected values for these quantities. Vertical blue lines indicate the beginnings of different laser bursts. Plots a), c), and e) were calculated using the downward slope of the absorption well, while plots b), d), and f) were calculated using the upward slope.

random noise, some bursts exhibit semi-periodic behavior. For example, the low-frequency-side measurements of bursts one and two in Figs. 6c and 6e exhibit oscillations with a period of approximately  $250 \mu\text{s}$ , but the same behavior is not observed in the same burst on the high-frequency-side measurements. Finally, no significant difference is observed between the high- and low-frequency-side measurements with these shock parameters. A summary of these performance metrics related to the shockwave is shown in Table 1. The accuracy of the velocity ratio ranges from 0.11 to 0.21 percent of the expected values, while the velocity difference accuracy ranges from 1.4 to 1.6 percent of the expected value.

Table 1: Summary of performance metrics of hybrid PB/CC-DGV in oblique-shock flowfield

Metric	$\varepsilon$ (down)	$\sigma$ (down)	$\varepsilon$ (up)	$\sigma$ (up)	$\varepsilon$ (combined)	$\sigma$ (combined)
$u_1$	6.0 m/s (1.0%)	10 m/s (1.7%)	5.0 m/s (0.8%)	9.5 m/s (1.6%)	5.5 m/s (0.9%)	9.8 m/s (1.6%)
$u_2$	5.9 m/s (1.0%)	9.6 m/s (1.6%)	4.9 m/s (0.8%)	9.1 m/s (1.6%)	5.9 m/s (1.0%)	9.3 m/s (1.6%)
$u_2/u_1$	0.002 (0.2%)	0.003 (0.3%)	0.001 (0.1%)	0.003 (0.3%)	0.001 (0.1%)	0.003 (0.3%)
$u_1 - u_2$	0.1 m/s (1.4%)	2.0 m/s (20%)	0.2 m/s (1.6%)	2.0 m/s (20%)	0.1 m/s (1.4%)	2.0 m/s (20%)

The earlier DGV work done by Herring et al. (Herring 2009) in the adjacent Test Section I of the same facility complex made comparison of pre- and post-shock velocities in a similar shock flowfield. Reported results showed an error in the measured velocity difference of 9 m/s, while the velocity ratio across the shock varied by 1.4 percent. These studies by Herring et al. also made use of instantaneous laser-induced thermal acoustics (LITA) in the same flowfield, finding measurement deviations of 8 m/s and 1.3 percent for the velocity difference and ratio, respectively. However, it was speculated in that work that the shock angle may not have been as expected, leading to a larger deviation than would otherwise have been the case. In comparison to these results, the hybrid PB/CC-DGV seems to measure the raw velocities and ratios more accurately, but perform with lesser precision, at least in considering the complete ensemble.

High-speed (50 kHz) DGV measurements by Saltzman et al. (Saltzman 2021) in a heated supersonic jet examined turbulent statistics and structure. These DGV measurements were able to make single-component velocity measurements within 2 percent of the jet core velocity, and RMS (fluctuating) velocity within 1 percent as compared to PIV measurements in the same jet. Measurements by Boyda and Lowe (Boyda 2018) using the original CC-DGV technique found RMS errors of 3 and 5 percent in laboratory-scale when comparing to pitot-probe measurements.

Additionally, the lab-scale tests done by Fahringer et al. (Fahringer 2020) in a low-speed jet indicated absolute velocity deviations around 5 m/s, or about 10 percent of the reference velocity in comparison with PIV measurements, and a velocity standard deviation in ambient air of about 3 m/s. Collectively, these data sets from the literature show the present hybrid PB/CC-DGV technique to perform similarly if not better than contemporary and historical techniques and applications.

These measurements and their characterization indicate the potential of this hybrid PB/CC-DGV technique for making both mean and instantaneous measurements. However, the flowfield examined in these studies is not ideal for an assessment of the unsteady properties since it was a steady laminar flow. Though the complete assessment of different flowfields is outside the scope of this paper, it will be of some value to show the kinds of flowfields that can be assessed with this technique. Figure 7 shows two different applications of hybrid PB/CC-DGV. Figures 7a and 7b show measurements made in a shock/boundary layer interaction beneath a concept reentry vehicle in a Mach 3.5 freestream previously studied with PB-CC-DGV. (Burns 2022 SciTech) In this flowfield, the bow shock from the model impinges on the floor boundary layer, leading to the formation of a separation shock. Figure 7a is the mean flowfield measured with PB-CC-DGV taken in a crossplane beneath the model showing the separation shock (large low-velocity region below  $y = 0.1$  m) as well as small shocklets emanating from control fins. In the mean, the separation shock has a smooth, curved appearance and a continuous, wall-normal, velocity gradient while approaching the floor. In contrast, the instantaneous flowfield in Fig. 7b shows many more complexities in the flow: the separation shock has more convolutions and irregularities, the area beneath the separation shock has alternating regions of high and low velocity, and the shocklets have similar irregularities to the separation shock. Background fluctuations can also be observed in the freestream flow. The Doppler shifts varied in these data from 100 to 400 MHz in the mean, but had mildly negative velocities in places, requiring a wide dynamic range. Also note that these data were taken at 25 kHz, but the procedure is identical.

Figures 7c and 7d show hybrid PB/CC-DGV measurements made in an atmospheric pressure, low-speed jet. This jet has a core velocity between 45 and 50 m/s and an exit diameter of 50 mm, similar to data previously reported by Fahringer. (Fahringer 2020) The mean velocity shown in Fig. 7c show some structure still present in the jet. Since this measurement took place over only 3 ms, much of the structure of this low-speed jet remains over the course of the measurement. The instantaneous field (Fig. 7d) shows more detail of this jet structure, including the subtle longitudinal variation in velocity associated with vortex shedding at the jet exit. The Doppler shifts present in these measurements range from 0 to 70 MHz. These two examples were selected because they represent significantly different ranges of measured Doppler shifts, both

from each other and from the oblique-shock test case (which had mean Doppler shifts ranging from 700 to 900 MHz). What these examples show is (1) the technique can be applied broadly to PB-CC-DGV datasets that have already been acquired and were not explicitly collected with this technique in mind, and (2) the technique maintains sufficient precision throughout a range of different conditions to make measurements possible even with relatively small or large Doppler shifts.

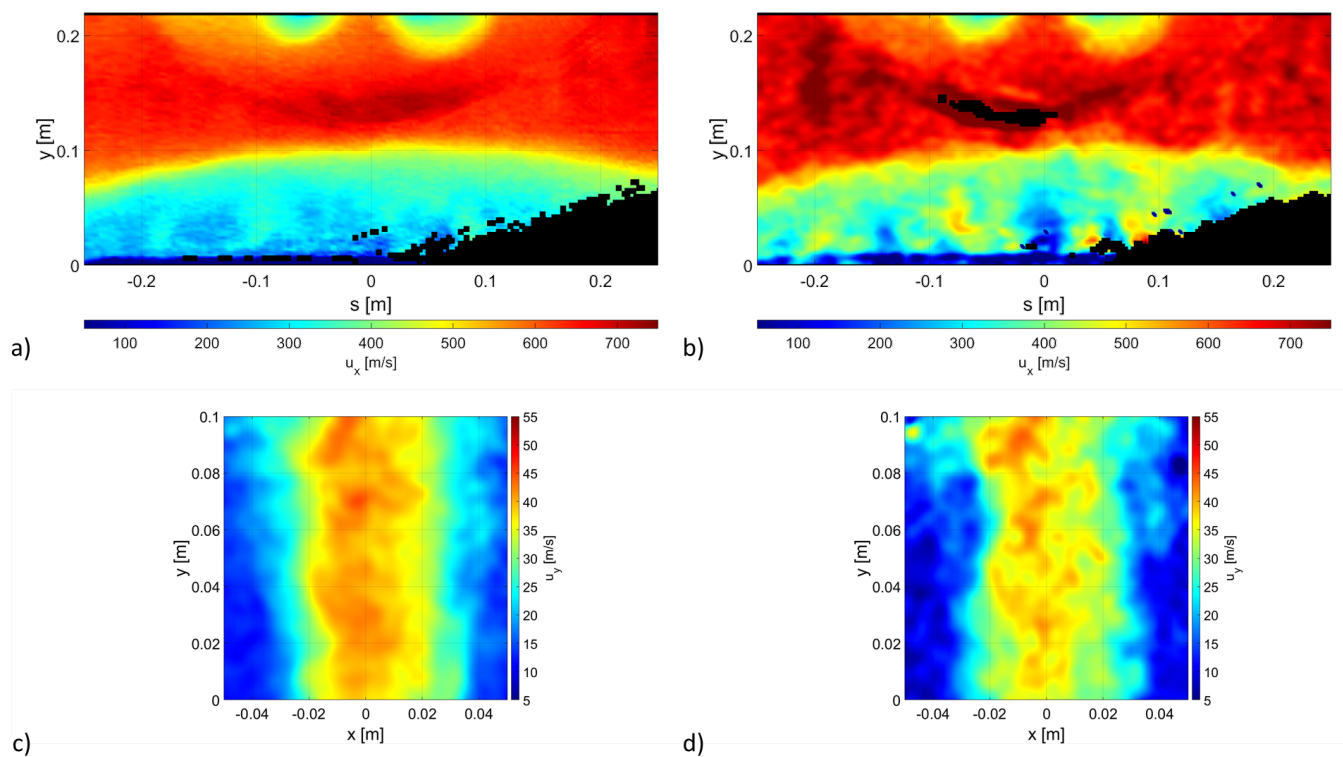


**Fig. 7** Other demonstrations of the h-PB/CC-DGV technique. a) and b) Sample single-burst mean (a) and instantaneous (b) velocity fields in a COBRA reentry vehicle flowfield, and c) and d) sample single-burst mean (c) and instantaneous (d) velocity fields in a low-speed jet.

These demonstrations, both the in-depth analysis of the oblique-shock flowfield and the simple demonstrations of the other flowfields, evoke fundamental questions about the utility of this technique. Notably, what is this technique for, and why would one opt to use this technique? This technique was conceived of as a means of extracting unsteady information from datasets intended to be mean measurements - measurements that had already been made. In this capacity, the appeal of this technique is that the data is 'free.' No additional measurements have to be made to make unsteady measurements. However, the limitations of the technique are also apparent. The contiguous datasets extracted in this way are currently limited to about 120 frames at 100 kHz. While this is sufficient for observing momentary unsteady phenomena, it is insufficient for gathering statistics regarding most frequency content and longer-period unsteady phenomena.

Comparatively, if one were to perform fixed-frequency DGV, datasets containing 1000 or more frames could be acquired in the same manner. While still not sufficient in record length for many circumstances, such a measurement would still provide a contiguous data trace over 8 times the length of those made available by the hybrid PB/CC-DGV technique, though they would likely not possess the dynamic or measurement range they hybrid technique provides. Moreover, optimizing the technique to improve the hybrid PB/CC-DGV (for example, increasing or decreasing the frequency scanning rate of the laser to yield more points that can be used with this technique) will have deleterious effects on the quality of the PB-CC-DGV on which the measurement is based. For these reasons, the niche for this technique is as previously described: to extract momentary unsteady information from measurements intended to be a mean.

Despite these limitations, the hybrid PB/CC-DGV technique has several functional advantages over traditional fixed-frequency DGV. Since the technique is rooted in the PB-CC-DGV technique, many of the advantages carry over to the hybrid technique including resistance to flatfield errors and laser frequency drifting. Moreover, resolving the complete absorption spectrum rather than looking at a subtly varying intensity ratio diminishes errors caused by incomplete knowledge of the local absorption topology and instrument miscalibration. Accordingly, higher-quality instantaneous velocity fields can be extracted with less complication to the experiment than fixed-frequency DGV. Finally, it bears repeating that this technique can be applied to previously-acquired datasets and any new measurements carried out with the PB-CC-DGV technique, without further complication to the experimental design or execution.

## 6. Conclusions

The hybrid pulse-burst/cross-correlation Doppler global velocimetry technique was demonstrated, making one-component velocity measurements at 100 kHz in an oblique shock flowfield. Measured instantaneous velocity fields appeared to have increased noise and lesser spatial homogeneity compared to the mean extracted through PB-CC-DGV. Examination of time-traces from these techniques showed similar but slightly diminished velocity accuracy and precision compared to the corresponding PB-CC-DGV measurements. These trends extended to the shock velocity ratio and difference. Ensemble measurement errors were found to be around 1-percent of local velocities with an accompanying measurement precision around 1.6 percent. Further demonstrations of the technique were made in a shock/boundary layer interaction flowfield and a low-speed jet. The hybrid PB/CC-DGV was able to resolve unsteady flow features not apparent in the mean, indicating the utility of this technique in flows possessing greater unsteadiness than the oblique shock. The technique, though able to make unsteady measurements, is limited due to the short contiguous time-traces it makes available. For this reason, the technique is best used for making momentary unsteady measurements rather than for detailed studies of

unsteady phenomena. However, the principal advantage of this technique is that it can be retroactively applied to previously-acquired datasets and datasets that have not been otherwise optimized for its use; it is essentially a free measurement to extract time-resolved instantaneous data from otherwise averaged data sets. This ability is an enormous strength that may make this technique appealing to researchers.

## Acknowledgements

The authors would like to thank the tunnel staff at the NASA Langley 4-Foot Unitary Plan Wind Tunnel for their help and cooperation in completing these tests. Additional thanks are given to Jim Ross for his continuing support of these research efforts. Funding for this work was through the NASA Aerosciences Evaluation and Test Capabilities (AETC) Portfolio and the NASA Transformational Tools and Technologies (TTT) program, Innovative Measurements discipline.

## References

- Boyda, M.T., & Lowe, K.T. (2018). Cross-Correlation Doppler Global Velocimetry using Rayleigh and Mie Scattering. In *AIAA 2018 Aerospace Sciences Meeting, Kissimmee, FL*.
- Burns, R.A, Fahringer, T.W., & Danehy, P.M. (2021). Velocity measurements across an oblique shock using pulse-burst cross-correlation DGV. In *AIAA SciTech 2021 Forum, Virtual Event*.
- Burns, R.A, Fahringer, T.W., & Danehy, P.M. (2022). Planar Investigation of a CobraMRV Reentry Flowfield Using Pulse-Burst, Cross-Correlation DGV. In *AIAA SciTech 2022 Forum, Dallas, TX*.
- Cadel, D.R. & Lowe, K.T. (2015). Cross-Correlation Doppler Global Velocimetry (CC-DGV). *Optics and Lasers In Engineering*, 71, 51-61.
- Charrett, T.O.H., Ford, H.D., Nobes, D.S., & Tatam, R.P. (2004), Two-Frequency Planar Doppler Velocimetry (2v-PDV). *Review of Scientific Instruments*, 75(11), 4487-4496.
- Fahringer, T.W., Burns, R.A., Danehy, P.M, Bardet, P.M., & Felver, J. (2020). Pulse-Burst Cross-Correlation Doppler Global Velocimetry. *AIAA Journal*, 58(6), 2364-2369.
- Fisher, A. (2017). Model-Based Review of Doppler Global Velocimetry Techniques with Laser Frequency Modulation. *Optics and Lasers In Engineering*, 93, 19-35.
- Forkey, J.N., Lempert, W.R., & Miles R.B. (1997). Corrected and calibrated I2 absorption model at the frequency-doubled Nd:YAG laser wavelengths. *Applied Optics*, 36(27), 6729-6738.
- Herring, G.C., Meyers, J.F., & Hart, R.C. (2009). Shock-strength determination with seeded and seedless laser methods. *Measurement Science and Technology*, 20(4).

- Lowe, K.T., Byun, G., Shea, S., Boyda, M., & Winski, C.S. (2019). Three-Velocity-Component Cross-Correlation Doppler Global Velocimetry for the Space Launch System Booster Separation Test in the NASA Langley Unitary Plan Wind Tunnel. In *AIAA 2019 Aviation Forum, Dallas, TX*.
- Meyers, J.F. (1995). Development of Doppler Global Velocimetry as a Flow Diagnostics Tool. *Measurement Science and Technology*, 6(6), 769-783.
- Müller, H., Eggert, M., Czarske, J., Büttner, L., & Fischer, A. (2007). *Experiments In Fluids*, 43(2), 223-232.
- Saltzman, A.J., Lowe, K.T., & Ng, W.F. (2021). 50 kHz Doppler global velocimetry for the study of large-scale turbulence In supersonic flows. *Experiments In Fluids*, 62.
- Saltzman, A.J., Beresh, S.J., Kearney, S.P., Crabtree, C.Q., and Slipchenko, M. (2022). Toward Snapshot Cross-Correlation Doppler Global Velocimetry for High-Speed Flows. In *AIAA Scitech 2022 Forum, Dallas, TX*.
- Thurrow, B.S., Jiang, N., Lempert, W.R., & Samimy, M. (2005). Development of Megahertz-Rate Planar Doppler Velocimetry for High-Speed Flows. *AIAA Journal*, 43(3), 500-511.